Int. J. Multiphase Flow Vol. 19, No. 4, pp. 665–681, 1993
Printed in Great Britain

0301-9322/93 $6.00 + 0.00
Pergamon Press Ltd

VELOCITY DISTRIBUTION FUNCTIONS FOR A BIDISPERSE, SEDIMENTING PARTICLE–GAS SUSPENSION

V. KUMARAN, H.-K. TSAO and D. L. KOCH
School of Chemical Engineering, Cornell University, Ithaca, NY 14853, U.S.A.

(Received 8 September 1992; in revised form 3 May 1993)

Abstract—The velocity distribution function of a dilute bidisperse particle–gas suspension depends on the relative magnitudes of the viscous relaxation time, τ_v, and the time between successive collisions, τ_c. The distribution functions in the two asymptotic limits, $\tau_c \ll \tau_v$ and $\tau_v \ll \tau_c$, which were analysed previously are qualitatively very different. In the former limit, the leading-order distributions are Gaussian distributions about the mean velocity of the suspension, whereas in the latter case the distributions for the two species are singular at their respective terminal velocities. Here, we calculate the properties of the suspension for intermediate values of τ_v/τ_c by approximating the distribution function as a composite Gaussian distribution. This distribution reduces to a Gaussian distribution in the limit $\tau_c \ll \tau_v$, in agreement with previous asymptotic analysis. In the intermediate regime, however, the composite Gaussian has a non-zero skewness, which is a salient feature of the distribution in the limit $\tau_v \ll \tau_c$. We have also performed numerical calculations using the direct-simulation Monte Carlo method. The approximate values for the moments of the velocity distribution obtained using the composite Gaussian compare well with the full numerical solutions for all values of τ_v/τ_c.

Key Words: sedimentation, fluidized bed, kinetic theory

1. INTRODUCTION

Particle–gas suspensions are encountered in many industrial processes, such as fluidized beds and pneumatic transport processes. The interaction between the particle and gas phases in the suspension is rather complex, and is influenced by the particle and gas inertia and gas viscosity, and the collisional and hydrodynamic interaction between the particles. Due to the complex nature of the interactions, it is difficult to calculate the macroscopic properties of the suspension from detailed microscopic models. Previous studies have used continuum models which treat the particle and gas as two continuous phases capable of exchanging momentum and energy.

The model that was used by Jackson (1963) to analyse the stability of a fluidized bed included particle inertia, and approximated the interaction between the fluid and particles by a drag force, $\mathbf{D} = \beta(n)(\mathbf{u} - \mathbf{v})$, where $\beta(n)$ is a function of the number density of the particles and $\mathbf{u}$ and $\mathbf{v}$ are the mean fluid and particle velocities, respectively. This analysis led to the conclusion that the uniform state of the fluidized bed is always unstable. More recent continuum theories (Didwania & Homsy 1982; Batchelor 1988) have attempted to improve on this model by incorporating the particle interactions in the form of a particle "pressure" and particle diffusivity, which are analogous to the pressure and diffusivity of the molecules in a gas. It has been speculated that the particle pressure could stabilize the uniform state of the fluidized bed. In the kinetic theory of gases, the pressure is proportional to the mean-square of the fluctuating velocity of the gas molecules, and it has been shown that the particle pressure can be related to the mean-square of the fluctuating velocities of the particles in rapid granular flows (Koch 1990; Jenkins & Richman 1985). However, the mean-square velocity is difficult to calculate in general because the distribution function of the particle velocities can be very different from the Maxwell–Boltzmann distribution for the molecules in an ideal gas.

The velocity distribution function for a dilute bidisperse particle–gas suspension settling in a quiescent gas in the limit $\mathrm{Re} \ll 1$ and $\mathrm{St} \gg 1$ was calculated in Kumaran & Koch (1993a, b), which hereafter will be referred to as parts 1 and 2, respectively. Here, the Reynolds number is given by $\mathrm{Re} = (\rho_G U a/\eta)$, and the Stokes number is given by $\mathrm{St} = [mU/(6\pi\eta a^2)]$, where ρ_G and η are the density and viscosity of the gas, m and a are the mass and radius of a particle and U is a characteristic velocity. The analysis is greatly simplified in this limit because for $\mathrm{Re} \ll 1$ the inertia

of the gas can be neglected, and the dominant effects in the suspension are the particle inertia and gas viscosity. The authors simplified the analysis further by neglecting the effect of hydrodynamic interactions and retaining only the collisional interactions between the particles; this approximation was shown to be valid for $\mathrm{St} \gg V^{-1/2}$ in the appendix to part 2, where V is the volume fraction of the particles. Hydrodynamic interactions play a significant role in the dynamics of monodisperse suspensions, which were analysed by Koch (1990).

The velocity fluctuations in a bidisperse suspension are controlled by a balance between the creation of fluctuating motion, due to solid–body interparticle collisions driven by the difference in the particles' terminal velocities, and the dissipation of this motion due to viscous drag. Therefore, there are two time scales that determine the dynamics of the bidisperse suspensions. The viscous relaxation time of species i, $\tau_{vi} = [m_i/(6\pi\eta a_i)]$ is the time it takes a particle to relax to its terminal velocity after a collision (see [3]). Here, m_i and a_i are the mass and radius of a particle of species i and η is the viscosity of the gas. The index i is used to denote the type of particle and in our convention, the index 1 is used for the heavier particle and 2 for the lighter particle. The collisional time, τ_{cij}, which is given by $[1/(n_j\pi d_{ij}^2 v_f)]$, is the time between successive collisions of a particle of species i with particles of species j (see [6]). Here, n_j is the number density of species j and v_f is the order of magnitude of the fluctuating velocity of the particles.

In parts 1 and 2, we analysed asymptotic limits in which one of the time scales is large compared to the other. In this paper, we calculate the moments of the velocity distribution in the intermediate region between the two limits using an approximate distribution function. In addition to this approximate calculation, we present values of the velocity moments derived from direct numerical simulations. For convenience, we define the parameter $\varepsilon_1 = [n_1(4\pi a_1^2)v_{1t}m_1/(6\pi\eta a_1)]$, which is proportional to the ratio of the collisional and viscous relaxation time for particles of species 1. Here, v_{1t} is the terminal velocity of particles of species 1, and we note that ε_1 is proportional to $\mathrm{St}V$, where V is the volume fraction of the particles and St, the Stokes number of particles of species 1, is given by $[m_1 v_{1t}/(6\pi\eta a_1^2)]$.

In the limit $\varepsilon_1 \gg 1$, which was analysed in part 1, the leading-order distribution functions of the two species are Gaussian distributions. The fluctuating velocities of the particles are $O(\varepsilon_1^{-1/3})$ smaller than the mean velocity. The velocity variances were calculated correct to $O(\varepsilon_1^{-2/3})$ from the balance equations for the velocity moments. The $O(\varepsilon_1^{-2/3})$ corrections to the velocity variances are small for ε_1 of $O(10^3)$, but they are of the same order of magnitude as the leading-order terms for ε_1 of $O(10^2)$, indicating that the asymptotic analysis is only accurate for very large values of ε_1. The mean-square velocity in the vertical direction in this limit, which is plotted on the right side of figure 1, shows a very sharp increase for ε_1 of $O(100)$.

In the limit $\varepsilon_1 \ll 1$, analysed in part 2, the particles relax to their terminal velocity between successive collisions, and the distribution function was calculated using a perturbation analysis about a base state in which all the particles are settling at their terminal velocities. The corrections to the mean and mean-square velocities of the particles are $O(\varepsilon_1)$ when scaled by the difference in terminal velocities. The $O(\varepsilon_1^2)$ corrections to the velocity moments are small for ε_1 of $O(0.1)$, indicating that the asymptotic analysis is quite robust in this limit and can be extended to higher values of ε_1.

It is useful to compare the mean velocity, velocity variance and skewness of the velocity distribution functions in the two limits. The skewness in the vertical direction is defined as $[\langle(v_{iz} - v_{im})^3\rangle/\langle(v_{iz} - v_{1m})^2\rangle^{3/2}]$, where v_{iz} and v_{im} are the particle velocity and the mean velocity of species i, and due to the symmetry of the system the skewness is zero in the horizontal plane. In the limit $\varepsilon_1 \gg 1$, the distribution function is an isotropic Gaussian and the skewness is zero to leading order. In the limit $\varepsilon_1 \ll 1$, the distribution is highly anisotropic and the mean-square velocity in the vertical direction is twice that in the horizontal plane. The skewness in the vertical direction increases as $\varepsilon_1^{-1/2}$ in this limit.

From figure 1, it can be seen that we do not have estimates for the mean-square fluctuating velocities in the intermediate region, which may be important in practical applications. For example, ε_1 is about 350 V for particles of 100 μm dia settling in air. Since exact solutions to the Boltzmann equation cannot be obtained except in the asymptotic limits, we must resort to either numerical simulations or an approximate analysis based on an assumed form of the distribution function. We shall pursue both of these approaches in the present paper. The numerical simulation

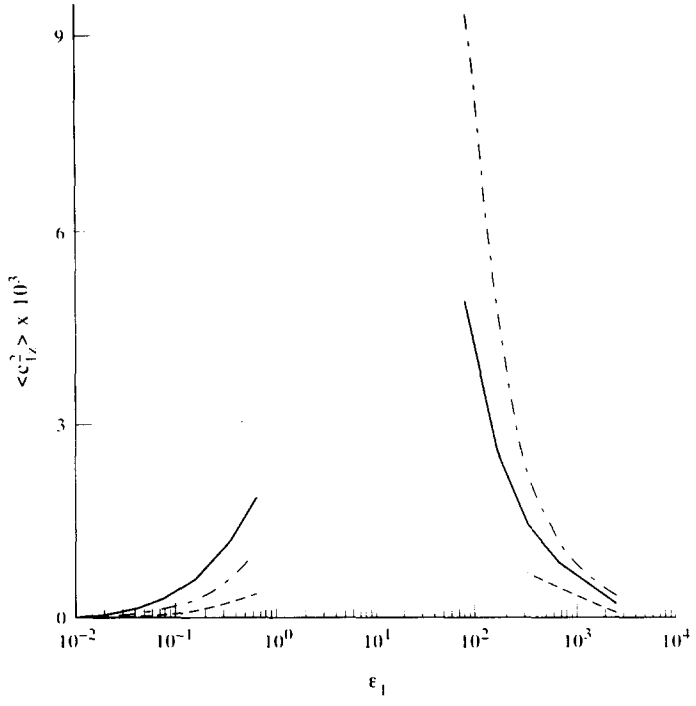

Figure 1. Mean-square of the fluctuating velocity in the vertical direction of the particles of species 1, as a function of ε_1. The curves on the left are the $\varepsilon_1 \ll 1$ asymptotic solutions calculated in part 2, and those on the right are the $\varepsilon_1 \gg 1$ asymptotic solutions calculated in part 1. The ratio of number densities, n_2/n_1, is 1 and the ratio of particle sizes, $a_c = a_2/a_1$, is: —·—, $a_c = 0.5$; ———, $a_c = 0.7$; – – – –, $a_c = 0.9$.

is based on the direct-simulation Monte Carlo (DSMC) method, which has been shown to be equivalent to a numerical solution of the non-linear Boltzmann equation (Bird 1970).

To obtain a theoretical model of the suspension dynamics in the intermediate region, we need an approximate distribution function that incorporates the characteristics of the distributions in the two limits. Since the analysis is less robust in the limit $\varepsilon_1 \gg 1$, we use a distribution function that is similar to a Gaussian in this limit, but has a non-zero skewness.

Distribution functions that are small perturbations about a Gaussian distribution have been used in the kinetic theory of dense gases, and in theories for granular flows. In the Chapman–Enskog theory for gas mixtures, the first perturbation to the distribution function is proportional to the gradients in the temperature and the mean velocities of the components (Chapman & Cowling 1970, Chap. 7). The coefficients of the gradient terms are expanded in a Sonine polynomial series, since the orthogonality of these polynomials simplifies the evaluation of the collision integral. The thermal conductivity and viscosity of the gas are determined from the first correction to the distribution function. However, this procedure is not appropriate for the present case for the following reasons. The analysis in kinetic theory uses a perturbation about the isotropic Maxwell–Boltzmann distribution, whereas in a bidisperse suspension we would expect the leading-order distribution function to be anisotropic and skewed in the intermediate regime. The forces on the particles are dependent on velocity, therefore the kinetic theory analysis gives an erroneous expression for the work done due to gravitational and viscous forces (see the end of the section 2.3 in part 1). Also, since the force is not divergence free in velocity space, the principle of detailed balancing is not applicable for these suspensions, as discussed in the appendix to part 1.

In granular flows there is a source of energy due to the shearing motion of the suspension, and the dissipation of energy due to viscous drag is assumed to be small compared to that due to inelastic collisions between particles (see Jenkins 1987). If the coefficient of restitution is close to 1, this system is similar to a dense gas of hard spheres in equilibrium, which has a Maxwell–Boltzmann distribution of velocities. The shearing of the suspension causes a perturbation to the leading-order distribution, and this is usually assumed to be an expansion in Hermite polynomials. Since the Hermite polynomials constitute an orthogonal function space, in which the inner product

is defined with a Gaussian weighting function, the moments of the distribution are relatively easy to calculate. However, this distribution function has the following disadvantage. If the highest power of the polynomial in the expansion is odd, the distribution function becomes negative at large velocities. For small perturbations, the fraction of particles having a negative distribution function is small, but for larger deviations from the Maxwell distribution this expansion assigns a negative distribution function to a significant fraction of the particles.

In section 2, we propose a composite Gaussian distribution that takes into account the skewness in the vertical velocity distribution, and is positive at all points in velocity space. The average properties calculated using this distribution function are compared to those obtained using asymptotic analysis in parts 1 and 2.

In section 3, we perform a numerical calculation of the error incurred in the equation for the velocity distribution function through the use of the approximate distribution function. This analysis provides a self-contained check on the validity of the approximation. In addition, we have verified the accuracy of the approximate calculation through a comparison with the results of numerical simulations, which are discussed in section 4.

2. APPROXIMATE DISTRIBUTION FUNCTION

We consider a uniform bidisperse suspension of particles of species 1 and 2, having masses m_1 and m_2, and radii a_1 and a_2, respectively, settling in a gas. The conservation equation for f_i, the distribution function of species i, is

$$\frac{\partial f_i}{\partial t} = -\nabla_{\mathbf{v}_i} \cdot \left(\frac{\mathrm{d}\mathbf{v}_i}{\mathrm{d}t} f_i(\mathbf{v}_i) \right) + \frac{\partial_c f_i}{\partial t}. \qquad [1]$$

Here, $\nabla_{\mathbf{v}_i}$ is the divergence operator in velocity space, and the first term on the right-hand side (RHS) is the accumulation of particles due to gravitational and drag forces. The acceleration of the particle due to these forces is given by

$$\frac{\mathrm{d}\mathbf{v}_i}{\mathrm{d}t} = \frac{v_{it}\mathbf{e}_z - \mathbf{v}_i}{\tau_{vi}}. \qquad [2]$$

Here v_{it} is the terminal velocity of particles of species i and $\mathbf{e}_z$ is the unit vector in the vertical direction; τ_{vi} is the viscous relaxation time, given by

$$\tau_{vi} = \frac{m_i}{6\pi\eta a_i}, \qquad [3]$$

where η is the viscosity of the gas.

The second term on the RHS of [1] is the collision integral or the rate of change of the distribution function due to collisions. For convenience, the collision integral is divided into two components:

$$\frac{\partial_c f_i}{\partial t} = N_i^{\mathrm{in}}(\mathbf{v}_i) - N_i^{\mathrm{out}}(\mathbf{v}_i). \qquad [4]$$

The collisional depletion of particles in the volume $\mathrm{d}\mathbf{v}_i$, due to collisions involving a particle in this volume, is calculated by carrying out an ensemble average over the velocities of the second particle in the collision and the orientations of the impact vector. Here, the impact vector is a vector joining the centers of the particles at the point of collision. The procedure for calculating the collisional depletion was described in part 1, and the final expression for $N_i^{\mathrm{out}}(\mathbf{v}_i)$ is

$$N_i^{\mathrm{out}}(\mathbf{v}_i) = \sum_{j=1}^{2} \frac{1}{\tau_{cij}} \int_{v_j} \int_{\eta=0}^{2\pi} \int_{\psi=0}^{\pi/2} f_i(\mathbf{v}_i) f_j(\mathbf{v}_j) w \cos\psi \sin\psi \, \mathrm{d}\psi \, \mathrm{d}\eta \, \mathrm{d}\mathbf{v}_j, \qquad [5]$$

where w is $|\mathbf{v}_i - \mathbf{v}_j|$, the magnitude of the relative velocity between the particles before collision. The time between successive collisions of a particle of species i with particles of species j, τ_{cij}, is given by

$$\tau_{cij} = \frac{1}{n_j(\pi d_{ij}^2) v_{\mathrm{r}}}. \qquad [6]$$

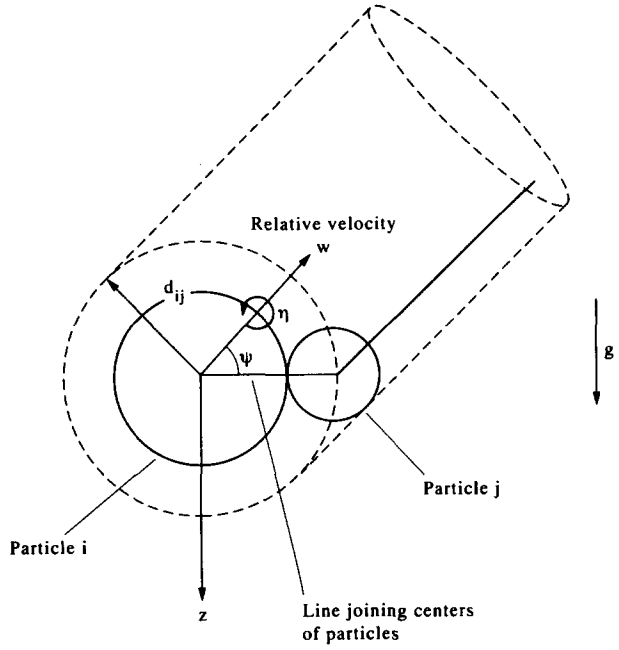

Figure 2. Collisional configuration for calculating the collisional accumulation and depletion.

Here v_f is the order of magnitude of the fluctuating velocity of the particles, which is the difference in terminal velocities for $\tau_v \sim \tau_c$. In [5], ψ and η are the azimuthal and meridional angles of the impact vector relative to the direction of the relative velocity, as shown in figure 2.

The collisional accumulation, $N_i^{in}(\mathbf{v}_i)$, in the volume $d\mathbf{v}_i$ is calculated by carrying out an ensemble average over all collisions that transport particles into this volume. The relations between the particle velocities before and after collision are given in section 2.4 in part 1, and the final expression for the collisional accumulation is

$$N_i^{in}(\mathbf{v}_i) = \sum_{j=1}^{2} \frac{1}{\tau_{cij}} \int_{\mathbf{v}_j^*} \int_{\eta=0}^{2\pi} \int_{\psi=0}^{\pi/2} f_i(\mathbf{v}_i^*) f_j(\mathbf{v}_j^*) w \cos\psi \sin\psi \, d\psi \, d\eta \, d\mathbf{v}_j^* . \quad [7]$$

Here, $\mathbf{v}_i^*$ and $\mathbf{v}_j^*$ are the velocities of the particles of species i and j before collision, w^* is the magnitude of the relative velocity between the particles before collision and the angles ψ and η are as defined before.

The approximate distribution function used in this paper is a composite Gaussian distribution of the form:

$$f_i(\mathbf{v}_i) = \frac{2}{\pi^{3/2}\xi_{ir}[\sqrt{\xi_{iz+}} + \sqrt{\xi_{iz-}}]} \exp\left[-\left(\frac{v_{ir}^2}{\xi_{ir}} + \frac{(v_{iz} - v_{is})^2}{\xi_{iz}} \right) \right], \quad [8]$$

where $\xi_{iz} = \xi_{iz+}$ for $v_{iz} > v_{is}$ and $\xi_{iz} = \xi_{iz-}$ for $v_{iz} < v_{is}$. This distribution function is shown in figure 3 for $v_{is} = 0$, $\xi_{iz+} = 1$ and $\xi_{iz-} = 0.5$. It consists of two Gaussian distributions patched together at

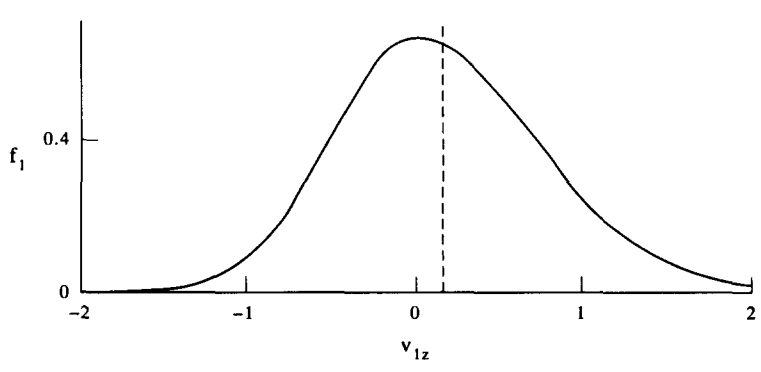

Figure 3. Distribution of vertical velocities for the composite Gaussian distribution. Here $v_{is} = 0$, $\xi_{iz+} = 1.0$ and $\xi_{iz-} = 0.5$. The dashed line represents the mean of the distribution.

their maximum and is continuous and differentiable about the plane $v_{iz} = v_{is}$. The distribution has a non-zero skewness in the vertical direction, and is always positive. Its second derivative is not continuous about the $v_{iz} = v_{is}$ plane, but this does not cause problems in the analysis since there are no second- or higher-order derivatives in the conservation equation. The moments of this distribution function, $\langle \beta_i(\mathbf{v}_i) \rangle$, are:

$$\langle v_{iz} \rangle = v_{is} + \frac{\xi_{iz+} - \xi_{iz-}}{\sqrt{\pi}\,[\sqrt{\xi_{iz+}} + \sqrt{\xi_{iz-}}]}, \qquad [9a]$$

$$\langle v_{iz}^2 \rangle = v_{is}^2 + \frac{\xi_{iz+} + \xi_{iz-} - \sqrt{\xi_{iz+}\xi_{iz-}}}{2} + \frac{2v_{is}(\xi_{iz+} - \xi_{iz-})}{\sqrt{\pi}\,[\sqrt{\xi_{iz+}} + \sqrt{\xi_{iz-}}]}, \qquad [9b]$$

$$\langle v_{ir}^2 \rangle = \xi_{ir} \qquad [9c]$$

and

$$\langle v_{iz}^3 \rangle = v_{is}^3 + \frac{3v_{is}^2(\xi_{iz+} - \xi_{iz-})}{\sqrt{\pi}\,[\sqrt{\xi_{iz+}} + \sqrt{\xi_{iz-}}]} - \frac{3v_{is}[\xi_{iz+} + \xi_{iz-} - \sqrt{\xi_{iz+}\xi_{iz-}}]}{2} + \frac{\xi_{iz+}^2 - \xi_{iz-}^2}{\sqrt{\pi}\,[\sqrt{\xi_{iz+}} + \sqrt{\xi_{iz-}}]}. \qquad [9d]$$

The parameters v_{is}, ξ_{ir}, ξ_{iz+} and ξ_{iz-} in a uniform suspension, at steady state, are calculated from the balance equations for the above moments:

$$\frac{\partial \langle \beta_i(\mathbf{v}_i) \rangle}{\partial t} = -\left\langle \left[\frac{d\mathbf{v}_i}{dt} \cdot \nabla_{\mathbf{v}_i} (\beta_i(\mathbf{v}_i)) \right] \right\rangle + \frac{\partial_c \langle \beta_i(\mathbf{v}_i) \rangle}{\partial t}. \qquad [10]$$

The collisional rate of change of the velocity moments are calculated using the ensemble-averaging procedure described in part 1. The steady-state values of the parameters v_{is}, ξ_{ir}, ξ_{iz+} and ξ_{iz-} are calculated by starting with an initial guess and integrating the unsteady-state balance equations in time until they converge to their final steady-state value.

The results that follow are for species 1, which is the heavier species in the suspension. Species 1 was chosen because it exhibits a larger deviation from the asymptotic solutions in the limit $\varepsilon_1 \gg 1$.

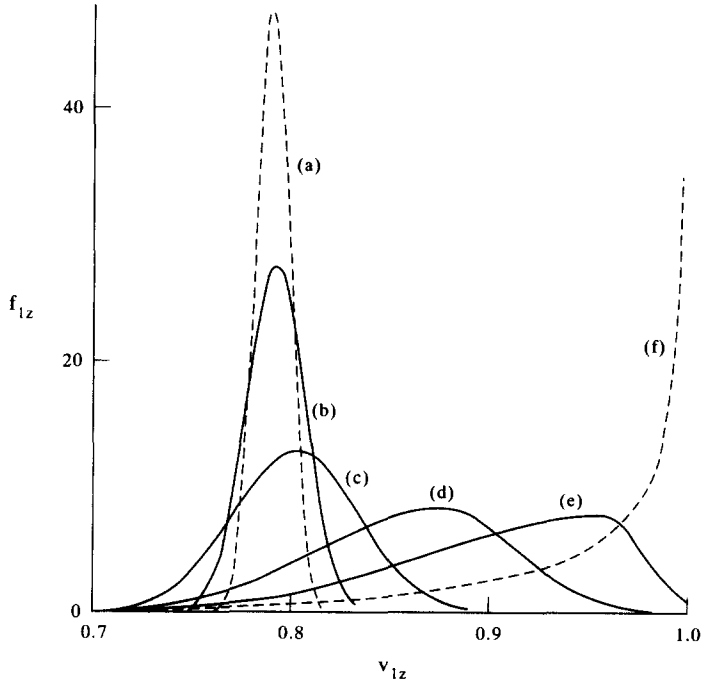

Figure 4. Distribution of vertical velocities $f_{1z}(v_{1z})$ as a function of vertical velocity v_{1z} for a particle size ratio $a_2/a_1 = 0.7$, and ratio of number densities $n_2/n_1 = 1$. The distribution functions represented by dashed lines were obtained using asymptotic analysis in the two limits. (a) $\varepsilon_1 = 10^4$ (asymptotic solution in the limit $\varepsilon \gg 1$); (b) $\varepsilon_1 = 10^3$; (c) $\varepsilon_1 = 10^2$; (d) $\varepsilon_1 = 8.779$; (e) $\varepsilon_1 = 2.601$; (f) $\varepsilon_1 = 0.5$ (asymptotic solution in the limit $\varepsilon_1 \ll 1$).

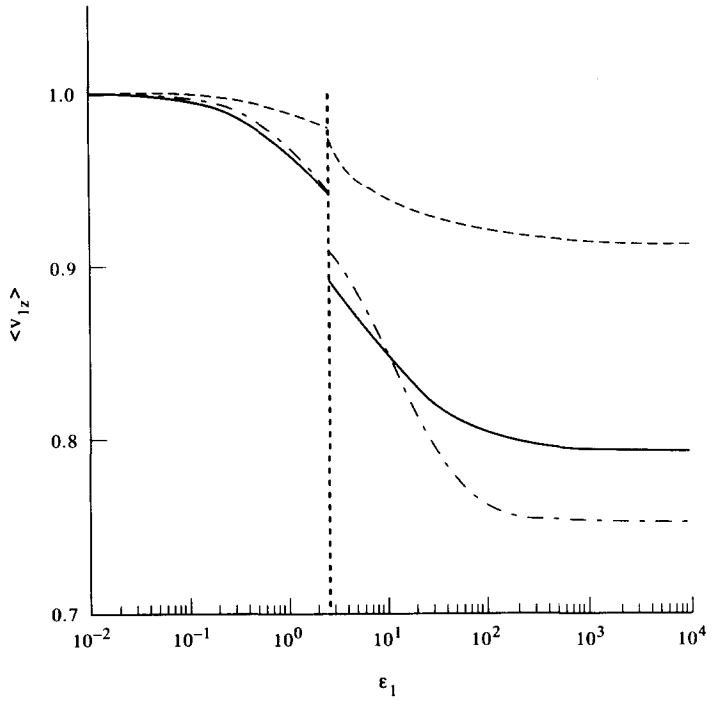

Figure 5. Mean velocity of species 1, $\langle v_{1z} \rangle$, as a function of ε_1. The curves on the left are the $\varepsilon_1 \ll 1$ asymptotic solutions and those on the right were obtained using the composite Gaussian distribution. The ratio of number densities, n_2/n_1, is 1, and the ratio of particle sizes, $a_c = a_2/a_1$, is: —·—, $a_c = 0.5$; ———, $a_c = 0.7$; - - - -, $a_c = 0.9$.

All velocities are non-dimensionalized by the terminal velocity of species 1, and a_c is the ratio of the radii of the two species, a_2/a_1. We present results for the case where the densities of the solid in the particles of the two species are equal, and their number densities, n_1 and n_2, are also equal.

The distribution of velocities in the vertical direction, $f_{iz}(v_{iz})$, is plotted as a function of the vertical velocity, v_{iz}, for various values of ε_1 in figure 4. Note that $f_{iz}(v_{iz})$ is the integral of the distribution function $f_i(\mathbf{v}_i)$ over the horizontal velocity coordinates. The distribution function for $\varepsilon_1 = 10^4$ was calculated using the asymptotic solution in the limit $\varepsilon_1 \gg 1$, and that for $\varepsilon_1 = 0.5$ was calculated using the asymptotic solution in the limit $\varepsilon_1 \ll 1$. The distribution of velocities for intermediate values of ε_1 were calculated using the composite Gaussian distribution. The results for this distribution could not be extended below $\varepsilon_1 = 2.5$, because the variance ξ_{iz+} decreases to zero at about this value. There is a smooth transition from the Gaussian to the composite Gaussian distribution as ε_1 is decreased from 10^4. But for small values of ε_1, the composite Gaussian distribution function is significantly different in form from the exact distribution in the limit $\varepsilon_1 \ll 1$, and the composite Gaussian is not singular at the terminal velocity.

The mean and mean-square velocities calculated using the composite Gaussian distribution are shown to the right of the dotted line in figures 5–7. The curves on the left of the dotted line were calculated using the analytical distribution function in the limit $\varepsilon_1 \ll 1$, and their accuracy at moderate values of ε_1 was enhanced by the inclusion of the $O(\varepsilon_1^2)$ corrections (see part 2). A comparison of figures 1 and 6, shows that the properties calculated using the composite distribution [8] are significantly different from those calculated using the large ε_1 asymptotic analysis, except at very large values of ε_1. (A comparison of figures 10–12 in part 2 with figures 5–7 in this paper also leads to the same conclusion.) The composite Gaussian distribution correctly captures the initial increase and subsequent decrease of the mean-square velocities as ε_1 is decreased, and its behaviour is similar to the $\varepsilon_1 \ll 1$ asymptotic solution at ε_1 of about 2.5.

Figure 8 shows the ratio of the mean-square velocities in the vertical and horizontal directions, $(\langle c_{iz}^2 \rangle / \langle c_{ir}^2 \rangle)$, which is a measure of the anisotropy in the velocity distribution. This ratio is 0.5 in the limit $\varepsilon_1 \gg 1$, since the leading-order distribution function is isotropic, and it is 2.0 in the other limit $\varepsilon_1 \ll 1$. The ratio calculated using the composite Gaussian distribution provides a smooth transition between the two limits.

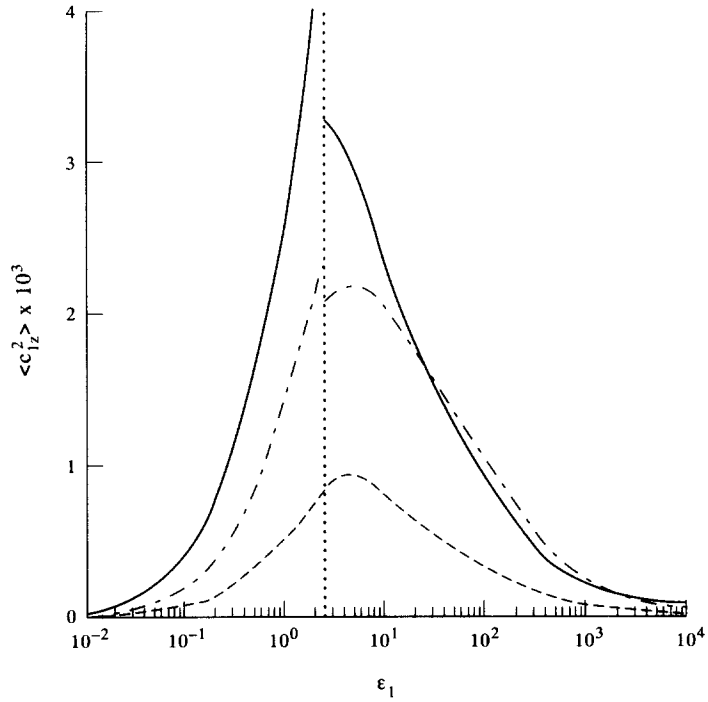

Figure 6. Mean-square of the vertical fluctuating velocity of species 1, $\langle c_{1z}^2 \rangle$, as a function of ε_1. The curves on the left are the $\varepsilon_1 \ll 1$ asymptotic solutions, and those on the right were obtained using the composite Gaussian distribution. The ratio of number densities, n_2/n_1, is 1, and the ratio of particle sizes, $a_c = a_2/a_1$, is: —·—, $a_c = 0.5$; ———, $a_c = 0.7$; – – – –, $a_c = 0.9$.

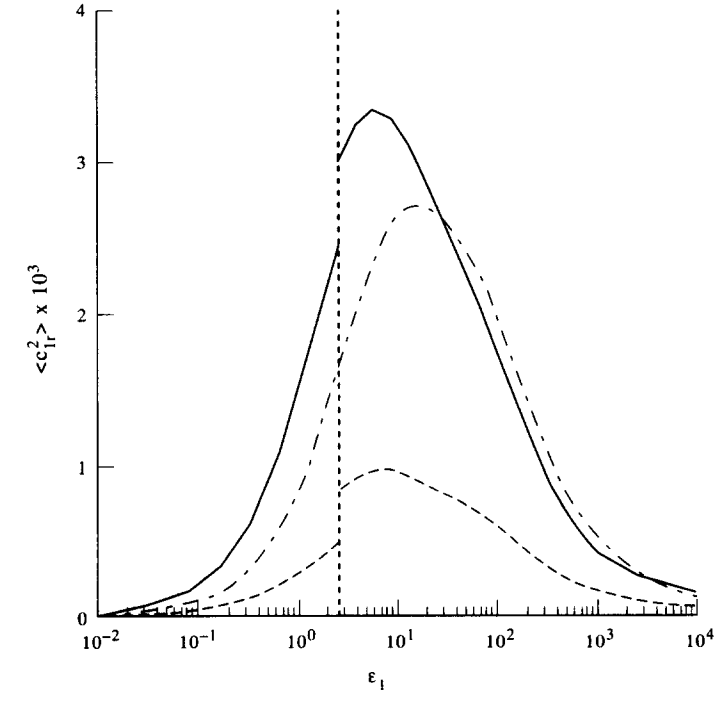

Figure 7. Mean-square of the horizontal fluctuating velocity of species 1, $\langle c_{1r}^2 \rangle$, as a function of ε_1. The curves on the left are the $\varepsilon_1 \ll 1$ asymptotic solutions, and those on the right were obtained using the composite Gaussian distribution. The ratio of number densities, n_2/n_1, is 1, and the ratio of particle sizes, $a_c = a_2/a_1$, is: —·—, $a_c = 0.5$; ———, $a_c = 0.7$; – – – –, $a_c = 0.9$.

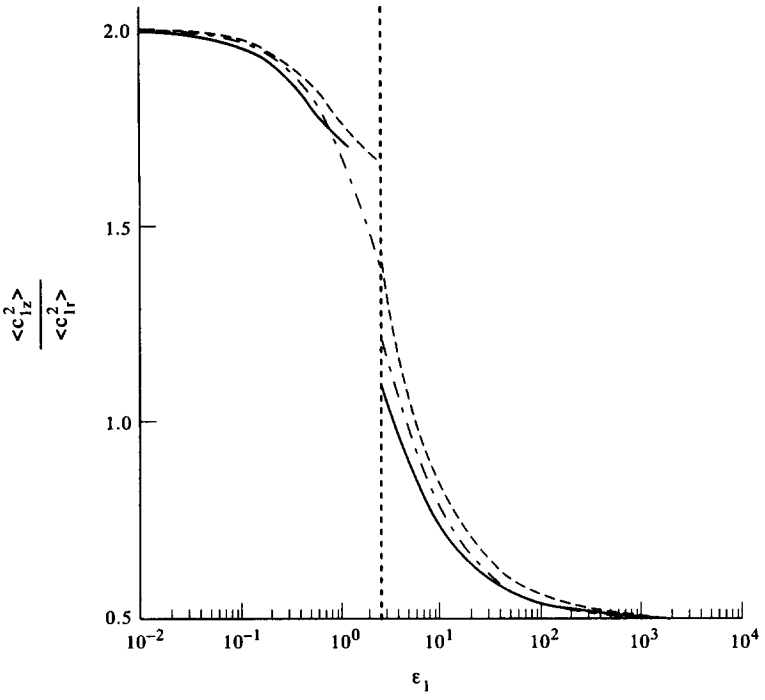

Figure 8. Ratio of the mean-square velocities in the vertical and horizontal directions ($\langle c_{1z}^2 \rangle / \langle c_{1r}^2 \rangle$), as a function of ε_1. The curves on the left are the $\varepsilon_1 \ll 1$ asymptotic solutions and those on the right were obtained using the composite Gaussian distribution. The ratio of number densities, n_2/n_1, is 1 and the ratio of particle sizes, $a_c = a_2/a_1$, is: —·—, $a_c = 0.5$; ———, $a_c = 0.7$; – – – –, $a_c = 0.9$.

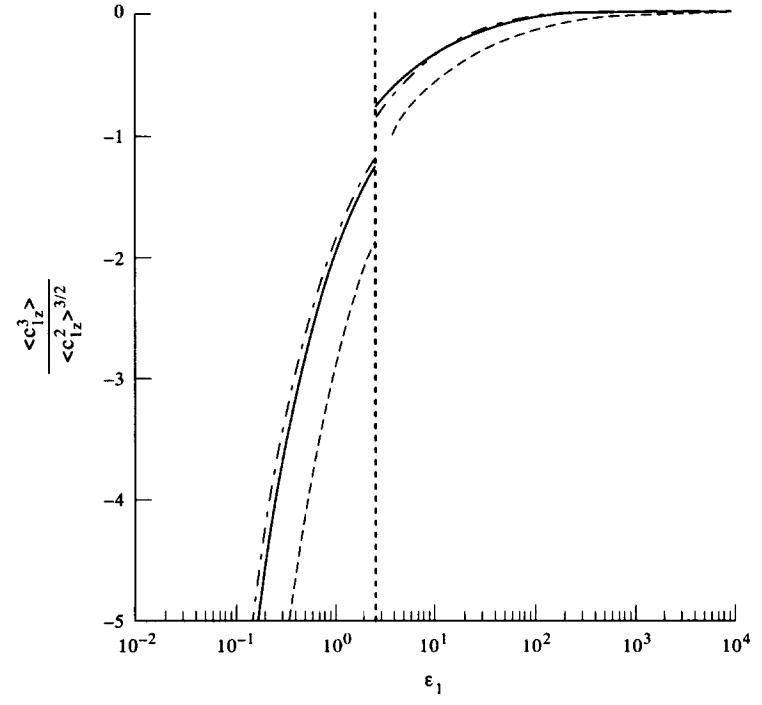

Figure 9. Skewness in the distribution of vertical velocities, ($\langle c_{1z}^3 \rangle / \langle c_{1z}^2 \rangle^{3/2}$), as a function of ε_1. The curves on the left are the $\varepsilon_1 \ll 1$ asymptotic solutions and those on the right were obtained using the composite Gaussian distribution. The ratio of number densities, n_2/n_1, is 1 and the ratio of particle sizes, $a_c = a_2/a_1$, is: —·—, $a_c = 0.5$; ———, $a_c = 0.7$; – – – –, $a_c = 0.9$.

Figure 9 is a plot of the skewness in the distribution of vertical velocities, which is defined as $[\langle c_{iz}^3 \rangle / \langle c_{iz}^2 \rangle^{3/2}]$. In the limit $\varepsilon_1 \gg 1$, the skewness is small since the leading-order distribution function is a Maxwellian. In the limit $\varepsilon_1 \ll 1$, the skewness increases as $\varepsilon_1^{-1/2}$, since both the second moment and third moment of the distribution are $O(\varepsilon_1)$. The skewness in the intermediate region, calculated using the composite Gaussian distribution, matches well with that calculated using asymptotic analysis in the limit $\varepsilon_1 \ll 1$. The skewness is small for ε_1 greater than about 100 and increases sharply to a value close to 1 as ε_1 is decreased to about 10.

The preceding results show that the composite Gaussian distribution gives more reasonable estimates for the velocity moments of the suspension than the asymptotic analysis used in part 1. Whereas the mean-square velocities calculated using the latter diverge for values of ε_1 as large as about 100, those calculated using the former give realistic results for ε_1 as low as about 2.5, and the values agree quite well with those calculated using asymptotic analysis in the limit $\varepsilon_1 \ll 1$. The improvement in the calculated properties more than makes up for the added complexity of including one additional conservation equation.

3. ACCURACY OF THE APPROXIMATE DISTRIBUTION FUNCTION

In this section, we estimate the accuracy of the composite Gaussian distribution. At steady state, the viscous and collisional accumulations, calculated using the exact solution to the conservation equation [1], sum to zero at every point in the velocity space:

$$N_i^{\text{in}}(\mathbf{v}_i) - N_i^{\text{out}}(\mathbf{v}_i) - \nabla_{\mathbf{v}_i} \cdot \left(\frac{\mathrm{d}\mathbf{v}_i}{\mathrm{d}t} f_i(\mathbf{v}_i) \right) = 0. \qquad [11]$$

Here, N_i^{in} is given by [7] and N_i^{out} is given by [5]. The parameters in the distribution function [8] were calculated by solving the four balance equations [10], and [8] is not the exact solution to the conservation equation. Therefore, it cannot be expected to give a zero net accumulation at every point in the velocity space.

We define a dimensionless measure of the accumulation error, $E_i(\mathbf{v}_i)$, as

$$E_i(\mathbf{v}_i) = \frac{N_i^{\text{in}}(\mathbf{v}_i) - N_i^{\text{out}}(\mathbf{v}_i) - \nabla_{\mathbf{v}_i} \cdot (\mathbf{v}_{i,t} f_i(\mathbf{v}_i))}{N_i^{\text{in}}(\mathbf{v}_i) + N_i^{\text{out}}(\mathbf{v}_i) + |\nabla_{\mathbf{v}_{i,t}} \cdot (\mathbf{v}_{i,t} f_i(\mathbf{v}_i))|}. \qquad [12]$$

E_i is zero at every point for the exact distribution function, and has a finite value at those points where the assumed distribution is in error. The root-mean-square of the accumulation error, averaged over velocity space, gives a measure of the closeness of the approximate distribution function to the exact distribution function. The mean-square of the error is

$$\langle E_i^2 \rangle = \int_{\mathbf{v}_i} (E_i(\mathbf{v}_i))^2 f_i(\mathbf{v}_i)\, \mathrm{d}\mathbf{v}_i. \qquad [13]$$

Since the exact distribution function is not known at this point, we use the composite Gaussian distribution as the weighting function in [13].

Numerical methods have been developed to solve the nonlinear Boltzmann equation for gas flows that are far from equilibrium (see Yen 1984). The numerical schemes consist of two steps: (i) a Monte Carlo method for calculating the collision integral; and (ii) a time integration scheme to calculate the final steady-state distribution. The equation is solved numerically over a finite volume in velocity space that is large enough to include most of the molecules. The value of the collision integral in each control volume is approximated by the product of the average of a large and random sample of the particle velocities and orientations at collision. This estimate of the collision integral is substituted into the integration scheme to obtain the value of the distribution function at the next time step.

In the present analysis, the collisional and viscous accumulations are calculated over a finite region in velocity space that is divided into control volumes. However, the collision integral is evaluated by a deterministic integration over the orientations and velocities of the particles at the point of collision. The viscous accumulation is calculated using a simple finite difference scheme. The mean-square of the accumulation error, $\langle E_i^2 \rangle$, is calculated by integrating the square of the accumulation error numerically over the velocity domain of species i.

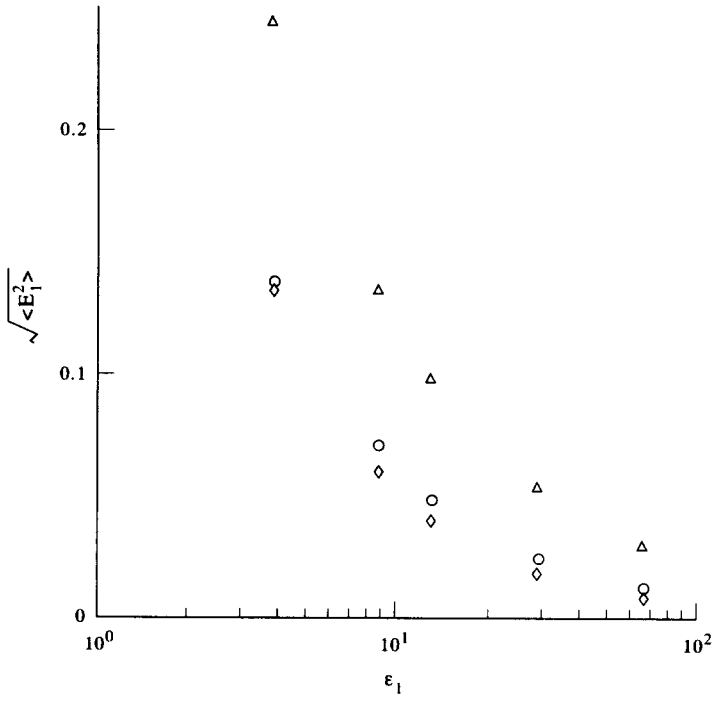

Figure 10. Root-mean-square accumulation error $\sqrt{\langle E_1^2 \rangle}$ as a function of ε_1. The ratio of number densities, n_2/n_1, is 1 and the ratio of particle sizes $a_c = a_2/a_1$, is: ◇, $a_c = 0.5$; ○, $a_c = 0.7$; △, $a_c = 0.9$.

A cylindrical coordinate system is employed over a finite domain in the velocity space of species i, which extends from 0 to $3.6\sqrt{\xi_{ir}}$ in the u_{ir} direction, and $-3.6\sqrt{\xi_{iz}}$ to $3.6\sqrt{\xi_{iz}}$ in the u_{iz} direction. Here, ξ_{iz} is the greater of ξ_{iz+} and ξ_{iz-}. The distribution function in this domain is specified at 325 nodes (13 equidistant values of u_{ir} each separated by $0.3\sqrt{\xi_{ir}}$ and 25 equidistant values of u_{iz} each separated by $0.3\sqrt{\xi_{iz}}$). Each of these nodes is at the center of a control volume. The viscous fluxes at each control surface are calculated using a 4-point interpolation scheme. The error due to the interpolation scheme is $< 1\%$ of the flux through the surface.

The collisional accumulation and depletion, which are given by [5] and [7], are five dimensional integrals over the coordinates v_{jr}, v_{jz}, ϕ, ψ and η. Here, ϕ is the polar angle between the horizontal velocities of parties i and j. These integrals are evaluated using a 12-point Gauss–Legendre quadrature for the ϕ, ψ and η coordinates, and a 12-point Gauss–Hermite quadrature for the v_{jr} and v_{jz} coordinates. The accuracy of the integration scheme was verified for a Gaussian velocity distribution, for which the collisional terms can be evaluated analytically. The results produced by the integration scheme had an error of about 2% for this distribution.

The root-mean-square of the accumulation error is plotted as a function of ε_1 in figure 10. The error is low for ε_1 greater than about 10, and at $\varepsilon_1 = 8$ the error is about 6% for $a_c = 0.5$ and 0.7, and close to 12% for $a_c = 0.9$. However, at $\varepsilon_1 = 2.5$, the error increases to about 12% for $a_c = 0.5$ and 0.7 and about 25% for $a_c = 0.9$. Thus, the assumed distribution function is accurate only for ε_1 greater than about 10.

4. NUMERICAL SIMULATIONS

In this section, we present results of numerical simulations for the moments of the velocity distribution in the bidisperse suspension. In a preliminary study, we used a dynamic simulation method, following changes in the position and velocity of N particles in a unit cell with periodic boundary conditions as they experienced solid–body collisions and a viscous drag force. This method gave accurate results for the collision dominated regime (large ε_1). However, when the viscous deceleration of the particles between each successive collision was large (small ε_1) and most of the particles had velocities close to their terminal velocities, the spatial configuration of the particles would arrange itself such that all the particles would miss one another and no further collisions would occur.

To avoid this situation, we decided to use the Direct-simulation Monte Carlo (DSMC) technique, which follows the evolution of the particles' velocity distribution functions in time without requiring the precise specification of particle positions. Bird (1970) has shown that the DSMC method is equivalent to a solution of the Boltzmann equation for a dilute suspension. The application of the technique to a bidisperse system is discussed in Bird (1968).

The DSMC method follows the evolution of the velocities of N_i particles of each species, where $N_i = 20{,}000$ for $i = 1, 2$ in most of our calculations. We choose a time step $\Delta t \ll \min(\tau_c, \tau_v)$, so the change in the velocity distribution functions within one time step is small. For small Δt, it is possible to decouple the effects of solid–body collisions and viscous drag on particle velocities. Thus, one first decelerates all particles due to viscous drag using [2]. Second, one calculates the effect of solid–body collisions using the following algorithm. Two particles are chosen at random and are accepted or rejected for a collision according to a probability weighting ($w\pi d_{ij}^2$) that is proportional to the collision rate calculated from their relative velocity and collision cross section, cf. [5]. If the pair is accepted, an impact parameter (ψ, η) is chosen with a probability weighting ($\cos\psi \sin\psi$) and the particle velocities are changed according to the rules for perfectly elastic, frictionless collisions. A set of time counters t_{ij} are kept for collisions between particles of species i and j and these are incremented by an amount

$$\Delta t_{ij} = \frac{1}{\pi d_{ij}^2 w}\left(\frac{1}{n_i N_j} + \frac{1}{n_j N_i}\right) \qquad [14]$$

following each successful ij-collision, where n_i and n_j are the number densities of species i and j. One continues to choose particles for collisions as described above until all of the time counters reach the next time increment and then the procedure of viscous relaxation and collision is repeated for the next time step. To obtain accurate results, it is required that the number of collisions occuring within the total set of particles in each time step is large and this can be achieved using large values of N_i.

Our simulation is simpler than the typical application of DSMC in rarefied gas dynamics in that we have a spatially homogeneous system. Thus, whereas one must typically discretize space and

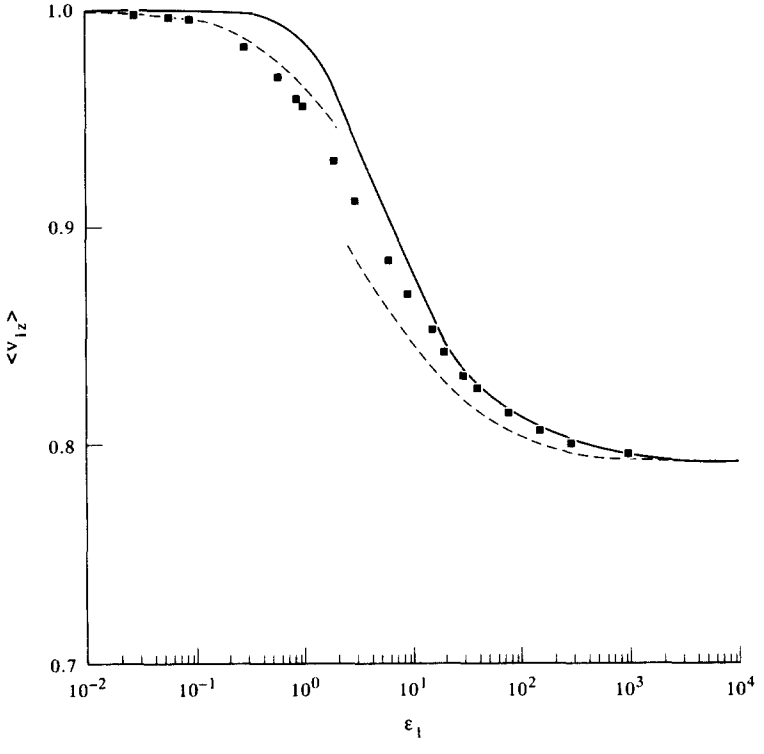

Figure 11. Mean velocity of species 1, $\langle v_{1z} \rangle$, as a function of ε_1: ■, DSMC numerical simulations; – – –, approximations described in section 2; ———, approximation of Goldman & Sirovich (1967). The ratio of particle number densities $n_2/n_1 = 1$ and the particle size ratio $a_2/a_1 = 0.7$.

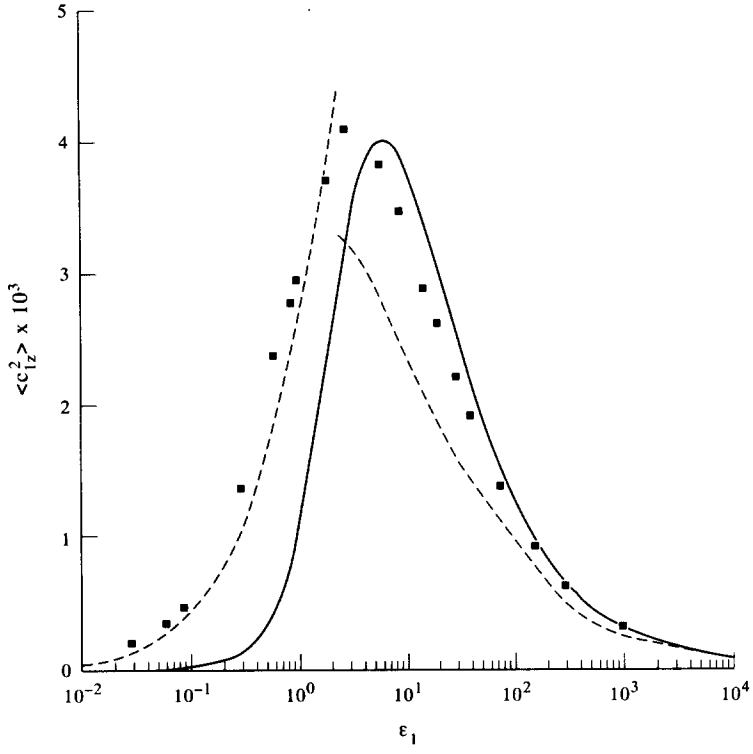

Figure 12. Mean-square of the vertical fluctuating velocity of species 1, $\langle c_{1z}^2 \rangle$, as a function of ε_1: ■, DSMC numerical simulations; – – –, approximations described in section 2; ———, approximation of Goldman & Sirovich (1967). The ratio of particle number densities $n_2/n_1 = 1$ and the particle size ratio $a_2/a_1 = 0.7$.

follow the velocity distribution function within a set of spatial cells by following the collisions between N_i particles within each cell, we need consider only one set of particles. This enables us to obtain accurate results for situations where the velocity distribution is far from a Maxwell distribution. For example, changing the number of particles of species 1 from 10,000 to 20,000 changes the results by $<0.2\%$ at $\varepsilon_1 = 3$.

As $\varepsilon_1 \to 0$ and the particles nearly relax to their terminal velocities between successive collisions, the number of 11- and 22-collisions becomes much smaller than the number of 12-collisions. This situation arises because the 12-collisions are driven by the differences in the particles' terminal velocities, whereas the *ii*-collisions require particles to deviate from their terminal velocities. As a result, it is difficult to obtain a large number of *ii*-collisions within a single time step for $\varepsilon_1 < 0.3$. The *ii*-collisions also have a relatively small effect on the velocity distribution in this limit, as may be seen from the analysis of part 2. Thus, we have neglected *ii*-collisions in the simulations for $\varepsilon_1 < 0.3$. A comparison of the calculation with and without *ii*-collisions for $\varepsilon_1 = 0.3$ shows that they cause 3.7 and 1.8% changes in the vertical and horizontal mean-square velocities, respectively, and this effect will become smaller as ε_1 is further decreased.

The results of the simulations are presented in figures 11–15. These figures give the moments of the distribution function of species 1 when the particles have equal density and the size ratio $a_2/a_1 = 0.7$. The solid squares represent the results of the simulation, the dashed lines are the results of the approximate calculations described in section 2 and the solid line is an approximation proposed by Goldman & Sirovich (1967), which will be described below. Figure 11 gives the mean velocity of species 1, figures 12 and 13 give the mean-square velocities in the vertical and horizontal directions respectively, figure 14 presents the ratio of the mean-square velocities and figure 15 the skewness. It may be seen that the approximations obtained in section 2 are close to the full numerical solutions for all values of ε_1 and for all moments considered. The maximum error incurred by using the small ε_1 asymptote for $\varepsilon_1 < 2.5$ and the composite Gaussian approximation for $\varepsilon_1 > 2.5$ as proposed in section 2 is about 20%. The comparison between the approximate

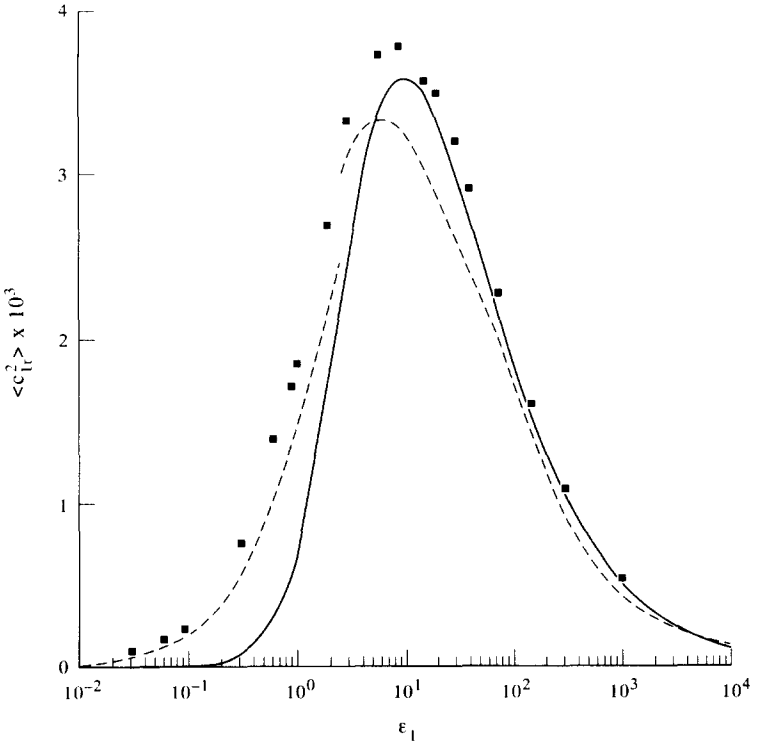

Figure 13. Mean-square of the vertical fluctuating velocity of species 1, $\langle c_{1r}^2 \rangle$, as a function of ε_1: ■, DSMC numerical simulations; – – –, approximations described in section 2; ———, approximation of Goldman & Sirovich (1967). The ratio of particle number densities $n_2/n_1 = 1$ and the particle size ratio $a_2/a_1 = 0.7$.

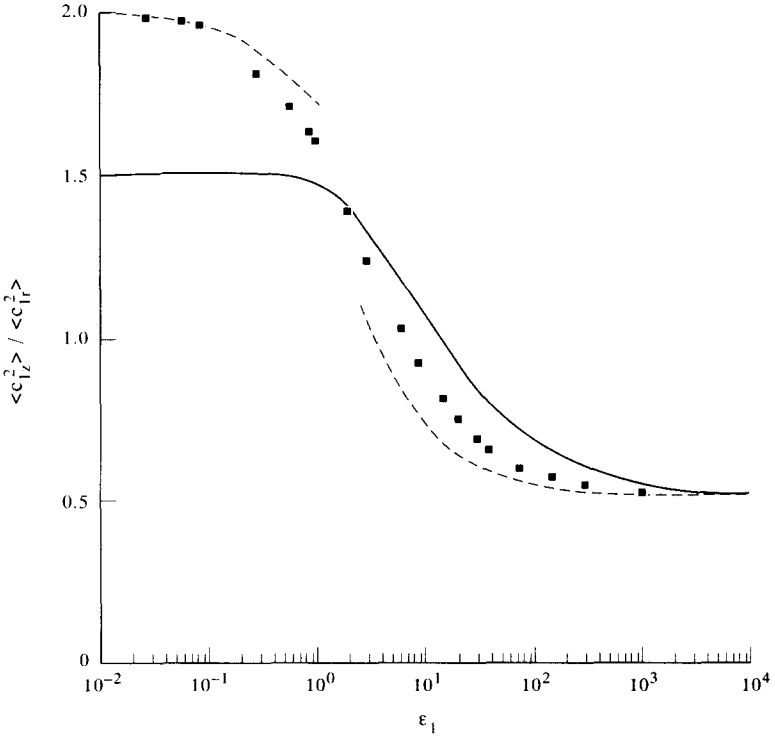

Figure 14. Ratio of the mean-square velocities in the vertical and horizontal directions of species 1, $(\langle c_{1z}^2 \rangle / \langle c_{1r}^2 \rangle)$, as a function of ε_1: ■, DSMC numerical simulations; – – –, approximations described in section 2; ———, approximation of Goldman & Sirovich (1967). The ratio of particle number densities $n_2/n_1 = 1$ and the particle size ratio $a_2/a_1 = 0.7$.

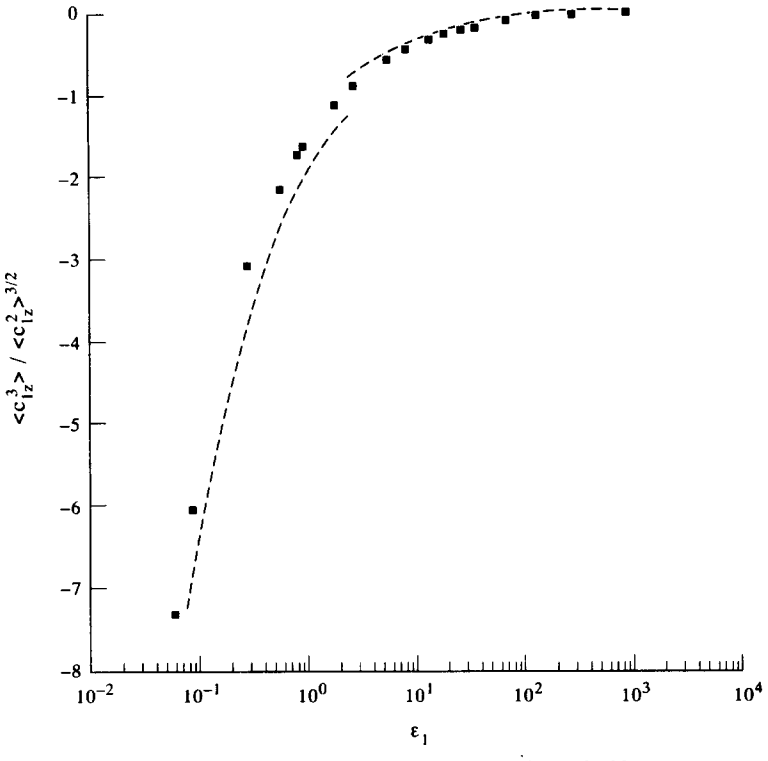

Figure 15. Skewness of the velocity distribution of species 1, $(\langle c_{1z}^3\rangle/\langle c_{1z}^2\rangle^{3/2})$, as a function of ε_1: ■, DSMC numerical simulations; – – – –, approximations described in section 2. The ratio of particle number densities $n_2/n_1 = 1$ and the particle size ratio $a_2/a_1 = 0.7$.

calculation and the numerical simulations is particularly good for $\varepsilon_1 \ll 1$ and $\varepsilon_1 \gg 1$, which is not surprising because the approximations are asymptotically valid in these limits.

A disadvantage of the approximate velocity distribution function that we have proposed is that we do not have a single expression for the distribution function that is valid for all ε_1. Instead we propose the use of the composite Gaussian distribution for $\varepsilon_1 > 2.5$. For smaller values of ε_1, this distribution function cannot be applied because one of the variances in the vertical direction goes to zero and instead we use the distribution function derived in part 2 for the limit $\varepsilon_1 \ll 1$. As discussed in the introduction, other proposed distribution functions give the aphysical result that the distribution function becomes negative over a substantial portion of the velocity space when the deviation from the Maxwell distribution is large. Goldman & Sirovich (1967) have proposed an approximate method for deriving the moments of the velocity distribution function without solving the full distribution function. This approximation neglects certain "off-diagonal terms" in the collision operator which couple the first and second moments to the higher moments of the velocity distribution function, and also makes certain approximations for the "diagonal terms" that are valid when the difference in the mean velocities of the two species is small compared to the root-mean-square velocity, i.e. $[\langle v_2 - v_1\rangle/\langle c_{1z}^2\rangle^{1/2}] \ll 1$. Goldman & Sirovich's (1967) approximation (solid lines) gives a single expression for all values of ε_1. However, their results for the mean-square velocities are inaccurate except at large values of ε_1 (see figures 12–14) and the ratio of the vertical to horizontal mean-square velocity given by Goldman & Sirovich's approximation as $\varepsilon_1 \to 0$ is 1.5 instead of the correct value of 2.0. The failure of the Goldman & Sirovich approximation for small ε_1 is not surprising in view of the fact that both the higher moments and the ratio $[\langle v_2 - v_1\rangle/\langle c_{1z}^2\rangle^{1/2}]$ become asymptotically large as $\varepsilon_1 \to 0$. These features make the development of approximate methods for determining the velocity distribution function for particulate flows much more difficult than for the molecular flows for which Goldman & Sirovich's approximation was originally intended.

5. CONCLUSIONS

In this paper, we calculated the velocity moments of the suspension between the two asymptotic limits analysed in parts 1 and 2. In the limit $\varepsilon_1 \ll 1$, the higher-order terms in the expression for the velocity moments were small compared to the leading-order terms for ε_1 as high as about 0.5. However, in the limit $\varepsilon_1 \gg 1$, the higher-order corrections were comparable to the leading-order velocity moments for ε_1 of about 100, indicating that the asymptotic analysis is not accurate for these values of ε_1. In this paper, the velocity moments in the intermediate region were calculated using a composite Gaussian distribution, which incorporates some of the features of the distributions in the two limits.

This distribution function reduces to the isotropic distribution in the limit $\varepsilon_1 \gg 1$, but it has a non-zero skewness in the vertical direction. It is simple in form, so that it is easy to numerically calculate collision integrals using Gauss–Hermite quadrature. Unlike perturbations to the Maxwell–Boltzmann distribution that are in the form of polynomial expansions, this function is positive at all points in the velocity space. It does not have a unique second derivative at its maximum point, but this does not affect the analysis because no derivatives of second or higher order are encountered in the conservation equation.

The parameters in the distribution function were calculated using balance equations for the following quantities for each species: (i) mean vertical velocity; (ii) mean-square of the vertical velocity; (iii) mean-square of the velocity in the horizontal plane; and (iii) third moment of the vertical velocity. The velocity moments were calculated for values of ε_1 as low as about 2.5 using the composite Gaussian distribution. At this point, one of the variances in the vertical direction became zero and the analysis could not be extended any further. For values of ε_1 smaller than 2.5, we proposed using the asymptotic results obtained in part 2 for $\varepsilon_1 \ll 1$.

In section 4, we presented results of numerical simulations for the moments of the velocity distribution in a bidisperse, sedimenting particle–gas suspension. These results were obtained using the DSMC technique. The results of the simulations and the approximate calculation were in good agreement for all values of ε_1 with the maximum deviation being about 20%. This finding is consistent with an independent error estimate for the composite Gaussian distribution given in section 3.

The mean velocity of species i varies from its terminal velocity for the viscous dominated case, $\varepsilon_1 \ll 1$, to a common mean velocity for the entire suspension in the collision dominated regime, $\varepsilon_1 \gg 1$. The mean-square velocity has a maximum value of $O(10^{-3})$ when ε_1 is $O(1)$ and approaches zero both as $\varepsilon_1 \to 0$ and as $\varepsilon_1 \to \infty$. For small values of ε_1 the viscous drag rapidly dissipates the kinetic energy of the particles. For large values of ε_1 the frequent collisions minimize the difference in the mean velocities of the two species and thereby decrease the source of particle energy. The skewness of the velocity distribution becomes quite large as ε_1 is decreased, and this feature is well-represented in both the composite Gaussian approximation and the numerical simulations.

The unusual features of the velocity distribution function for the particulate suspension in cases where the dissipative effects of the viscous drag forces are significant present challenges for the kinetic theory. It is important to choose an approximate form for the velocity distribution function and a method of analysis that captures the salient features of the specific flow problem being addressed.

Acknowledgements—The authors thank James T. Jenkins for many helpful discussions. This work was supported by grant CTS-885 7565 from the National Science Foundation Fluids, Particulates and Hydraulics Program. The numerical calculations were performed using the Cornell National Supercomputer Facility, which is supported by the NSF and IBM Corporation.

REFERENCES

BATCHELOR, G. K. 1988 A new theory for the instability of a fluidized bed. *J. Fluid Mech.* **193,** 75–110.

BIRD, G. A. 1968 The structure of normal shock waves in a binary gas mixture. *J. Fluid Mech.* **31,** 657–668.

BIRD, G. A. 1970 Direct simulation and the Boltzmann equation. *Phys. Fluids* **13,** 2676–2681.

CHAPMAN, S. & COWLING, T. G. 1970 *The Mathematical Theory of Non-uniform Gases.* Cambridge University Press, New York.

DIDWANIA, A. K. & HOMSY, G. M. 1982 Resonant sideband instabilities in wave propagation of fluidised beds. *J. Fluid Mech.* **122,** 433–438.

GOLDMAN, E. & SIROVICH, L. 1967 Equations for gas mixtures. *Phys. Fluids* **10,** 1928–1940.

JACKSON, R. 1963 The mechanics of fluidized beds. Parts 1 and 2. *Trans. Instn Chem. Engrs* **41,** 12–28.

JENKINS, J. T. 1987 Balance laws and constitutive relations for rapid flows of granular materials. In *Constitutive Models of Deformation* (Edited by CHANDRA, R. & SRIVASTAVA, R.). SIAM, Philadelphia, PA.

JENKINS, J. T. & RICHMAN, M. W. 1985 Kinetic theory for plane flows of a dense gas of identical, rough, inelastic circular disks. *Phys. Fluids* **A28,** 3485–3494.

KOCH, D. L. 1990 Kinetic theory for a monodisperse gas–solid suspension. *Phys. Fluids* **A2,** 1711–1723.

KUMARAN, V. & KOCH, D. L. 1993a Properties of a bidisperse particle–gas suspension. Part 1: collision time small compared with viscous relaxation time. *J. Fluid Mech.* **247,** 623–641.

KUMARAN, V. & KOCH, D. L. 1993b Properties of a bidisperse particle–gas suspension. Part 2: viscous relaxation time small compared with collision time. *J. Fluid Mech.* **247,** 643–660.

YEN, S. M. 1984 Numerical solution of the nonlinear Boltzmann equation. *A. Rev. Fluid Mech.* **16,** 67–97.